



Water soluble PEGylated phenothiazines as valuable building blocks for bio-materials

Sandu Cibotaru^a, Andreea-Isabela Sandu^a, Dalila Belei^b, Luminita Marin^{a,*}

^a "Petru Poni" Institute of Macromolecular Chemistry of Romanian Academy, Iasi, Romania

^b "Alexandru Ioan Cuza" University, Department of Organic Chemistry, Iasi, Romania

ARTICLE INFO

Keywords:

Phenothiazine
Poly(ethylene glycol)
Luminescence
Biocompatibility
Antitumor activity
Aggregation induced emission

ABSTRACT

The paper reports a series of three new PEGylated phenothiazine derivatives which keep the potential of valuable building blocks for preparing eco-materials addressed to a large realm of fields, from bio-medicine to opto-electronics. They were synthesized by connecting the hydrophilic poly(ethylene glycol) to the hydrophobic phenothiazine via an ether, ester, or amide linking group. The successful synthesis of the targeted polymers and their purity were demonstrated by NMR and FTIR spectroscopy methods. Their capacity to self-assembly in water was studied by DLS and UV-vis techniques and the particularities of the formed aggregates were investigated by fluorescence spectroscopy, SEM, AFM, POM and UV light microscopy. The biocompatibility was assessed on normal human dermal fibroblasts and human cervical cancer cells. The synthesized compounds showed the formation of luminescent aggregates and proved excellent biocompatibility on normal cells. In addition, a concentration dependent cytotoxicity against HeLa cancer cells was noticed for the PEGylated phenothiazine containing an ester unit.

1. Introduction

Phenothiazine is a valuable building block for the synthesis of a wide range of compounds useful in various domains, from optoelectronics [1] to medicine [2]. The high potential for such diverse applications is supported by its chemical structure and the ability to promote supramolecular assembly. Phenothiazine is a fused tricyclic system, with two heteroatoms on the median axis of the central ring. This results in a bent shape, known as „butterfly geometry”, which impacts the supramolecular self-assembling of the compounds containing it, usually involving large inter-molecular distances. The two heteroatoms ensure a strong electron-donor character, which is exploited in the synthesis of donor-acceptor systems with extended electron delocalization and good charge mobility, property required for the active substrate in the organic solar cells, field effect transistors (OFETs) and light emitting diodes (OLEDs). The large intermolecular distances facilitate the luminescence in solid state, property required by the OLED materials, as they hinder the luminescence quenching by excimer formation [3].

In medicine, phenothiazine demonstrated a versatile biological activity, being used in the synthesis of many classes of drugs, such as bactericides, fungicides, antitumor, antiviral, anti-inflammatory, anti-malarial, antifilarial, trypanocidal, anticonvulsant, analgesic and immunosuppressive agents [4]. For cancer therapy, the phenothiazine-

based derivatives already proved selective efficiency towards several cancer lines [2]. Due to their high bioactivity, they are promising as multifunctional drugs in the palliative therapy of the cancer patients; its analgesic and antipsychotic activity can overcome the side effects of chemotherapy, such as nausea or vomiting [5].

The main drawback of the phenothiazine derivatives is their low solubility in environmental friendly solvents or water bio-dispersant [6]. This limits their bioavailability in bio-applications and the ability to be manufactured as solid materials for optoelectronics. The use of highly polar solvents generates high amounts of residual toxic pollutants, which are hazardous for environment and threatening for the health [7]. This issue was partially addressed by grafting hydrophobic chains at the phenothiazine nitrogen or bulky units on the phenothiazine core [8]. For instance, improved water solubility was attained using diethanolamine [9] or quaternary ammonium salts [10] as grafting groups. Few recent studies reported excellent water solubility by grafting ethylene oxide units at the nitrogen atom of phenothiazine [11,12] or inserting poly(ethylene glycol) in the main backbone [13], but no linkage of the poly(ethylene glycol) as lateral chain of phenothiazine was reported so far. The experience of our group in the phenothiazine domain made us aware of the challenges raised by the phenothiazine insolubility for real world applications [14–20]. To overcome this issue we designed a material consisting of the

* Corresponding author.

E-mail address: lmartin@icmpp.ro (L. Marin).

<https://doi.org/10.1016/j.msec.2020.111216>

Received 29 January 2020; Received in revised form 21 May 2020; Accepted 18 June 2020

Available online 20 June 2020

0928-4931/ © 2020 Elsevier B.V. All rights reserved.

hydrophobic phenothiazine heterocycle and hydrophilic units. To reach this aim we selected the poly(ethylene glycol) (PEG), a water soluble, biocompatible polymer approved by US-FDA, which is frequently used for bio-applications, especially for gene therapy [21,22], tissue engineering [23] and drug formulations [24–27]. Its successful use for bio-applications is further supported by other properties, such as non-toxicity, biologic inertness, resistance to protein adsorption, while it is easily eliminated either by renal or hepatic pathways [28].

Having in mind this state of the art, we designed and synthesized new PEGylated phenothiazine compounds by connecting the two units (*i.e.* phenothiazine and PEG) *via* an ether, ester, or amide linking group. The design took into consideration the valuable properties of the units, which keep the promise to yield valuable building blocks for bio-applications and ecological opto-electronic materials as well. Amide or ester linking units were selected aiming to achieve well-ordered supramolecular assemblies [29,30] and to confer ability of molecular recognition of the biomolecules of human body [31]. The purification method of the targeted compounds was optimized to provide pure samples with high yield.

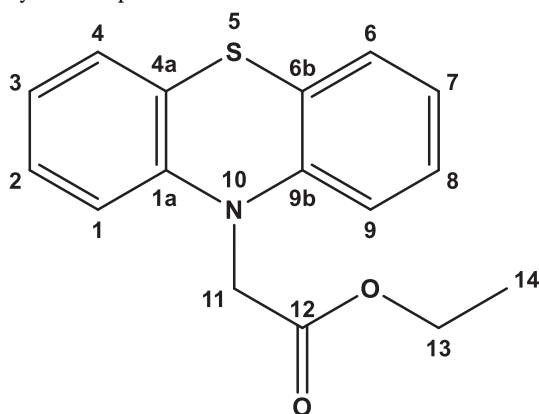
2. Experimental

2.1. Materials

Phenothiazine 98%, ethyl bromoacetate 98%, sodium hydride 95%, methoxy poly(ethylene glycol) (550 Da, polymerization degree:11–13), *p*-toluenesulfonyl chloride 98%, pyridine 99.8%, trimethylamine (TEA) 99%, *N*-hydroxysuccinimide (NHS) 98%, *N*-(3-dimethylaminopropyl)-*N'*-ethylcarbodiimide hydrochloride (EDC.HCl) 98% were purchased from Aldrich; sodium hydroxide 97% and methoxy poly(ethylene glycol) amine (750 Da, polymerization degree:16–18) were from Fluka and 4-(dimethylamino)-pyridine was from Merck. All the reagents and solvents were used as received.

2.2. Synthesis

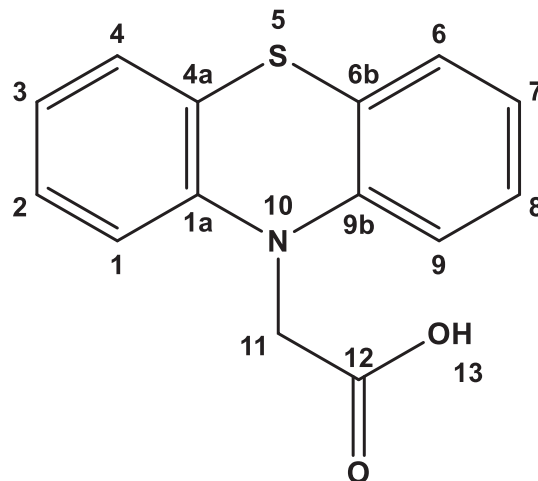
2-(10H-phenothiazin-10-yl) ethyl acetate (PACoEt) was synthesized by *N*-alkylation of phenothiazine.



The synthesis was realized following a slightly modified literature protocol [32,33]. In a Schlenk tube placed on an ice bath, were introduced 0.8 g NaH (1.5 eq), 2.8 g K₂CO₃ (1 eq) and 30 mL DMF, under nitrogen atmosphere and magnetic stirring. After 10 min, when the mixture reached 0 °C, a solution of 4 g phenothiazine (1 eq) in 10 mL DMF was added and the obtained reaction mixture was maintained under vigorous stirring for 30 min. Then 4.6 mL of ethyl bromoacetate (2 eq) was slowly dropwise during 10 min, and the obtained solution was allowed to reach room temperature and kept under vigorous magnetic stirring. After 23 h, the reaction mixture was precipitated in water, and the crude product was filtered and purified by recrystallization from ethanol, when 7.3 g product was dissolved in

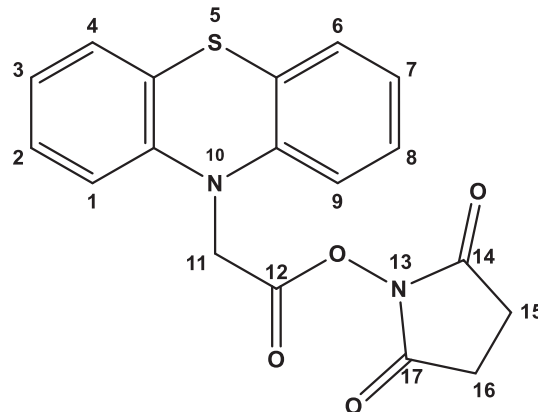
100 mL ethanol at 60 °C under magnetic stirring, kept for 30 min to appear the crystals, and then filtered again, when colourless crystals were obtained. $\eta = 66\%$; mp 101–103 °C. ¹H NMR (400 MHz, DMSO-*d*₆, ppm) $\delta = 7.17$ – 7.12 (m, 4H, H1, H2, H8, H9), 6.97–6.93 (t, 2H, H3, H7), 6.69; 6.67 (d, 2H, H4, H6), 4.67 (s, 2H, H11), 4.26–4.21 (q, 2H, H13), 1.28–1.24 (t, 3H, H14); ¹³C NMR (100 MHz, DMSO-*d*₆, ppm) $\delta = 169.98$ (C12), 144.21 (C1a,9b), 127.40 (C1, 9), 127.07 (C2,8), 123.42 (C4a, 6b), 123.05 (C4, 6), 114.62 (C3, 7), 61.68 (C13), 51.09 (C11), 14.31 (C14); FT-IR (KBr, cm⁻¹): 3008 (ν CH aromatic), 2931 (ν CH aliphatic), 1727 (ν C=O), 1589, 1566 (ν C=C), 1216 (ν C-O-C), 857, 749, 710 (δ C-H).

2-(10H-phenothiazin-10-yl) acetic acid (PACoH) was prepared by a saponification reaction of the phenothiazine ester, following a reported procedure [32].



In a round bottom flask were introduced 2 g PACoEt (1 eq), 1.75 mL sodium hydroxide 40% (3.5 eq) and 20 mL methanol, under vigorous stirring, at 60 °C. After 4 h, the reaction mixture was cooled down to room temperature, and then 30 mL of HCl 0.5 M was added to decrease pH to 5–4, when a white precipitate was obtained. The crude product was filtered and dried 24 h under vacuum to give a grey powder. $\eta = 91$; mp = 189–190 °C. ¹H NMR (400 MHz, DMSO-*d*₆, ppm) $\delta = 13.1$ (s, 1H, H13), 7.18–7.10 (m, 4H, H1, H2, H8, H9), 6.96–6.92 (t, 2H, H3, H7), 6.71; 6.70 (d, 2H, H4, H6), 4.56 (s, 2H, H11); ¹³C NMR (100 MHz, DMSO-*d*₆, ppm) $\delta = 170.85$ (C12), 143.83 (C1a, 9b), 127.53 (C1, 9), 126.58 (C2,8), 122.73 (C4, 6), 121.40 (C4a, 6b), 114.98 (C3, 7), 49.70 (C11); FT-IR (KBr, cm⁻¹): 3340 (ν O-H), 3095–3066 (ν CH aromatic), 2962–2935 (ν CH aliphatic), 1760, 1701 (ν C=O), 1593, 1571 (ν C=C), 1465 (δ CH₂), 1442, 1425(δ O-H), 1226, 1211 (ν C-N).

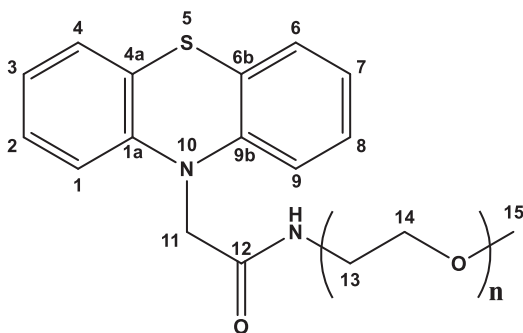
2,5-Dioxopyrrolidin-1-yl 2-(10H-phenothiazin-10-yl)acetate (PACoS) was prepared by a phenothiazine activated ester synthesis [32].



In a plate bottom flask, 1 g of PACoH (1 eq) was dissolved in 17 mL dichloromethane under magnetic stirring, and then mixed with 0.9 g of

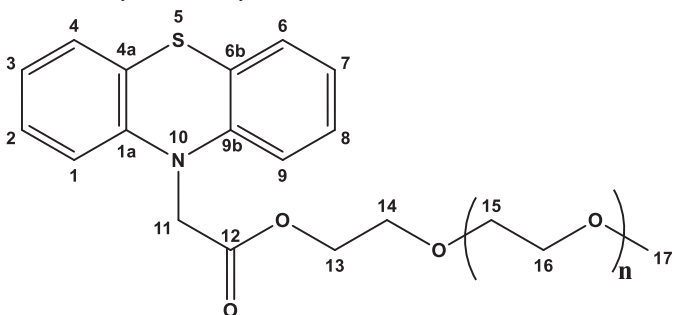
1-ethyl-3-(3-dimethylaminopropyl) carbodiimide (EDC.HCl) (1.2 eq). After 15 min, when the mixture became a clear solution, 0.55 g *N*-hydroxysuccinimide (NHS) (1.2 eq) was added, and the reaction mixture was maintained 24 h under stirring at room temperature. Further, the solution was dried with $MgSO_4$, filtered, and the solvent was removed under reduced pressure. The solid compound was recrystallized from methanol to give slight pink crystals. $\eta = 65\%$; mp = 167–169 °C; 1H NMR (400 MHz, $DMSO-d_6$, ppm) $\delta = 7.21-7.17$ (t, 4H, H1, H2, H8, H9), 7.02–6.98 (t, 2H, H3, H7), 6.82; 6.80 (d, 2H, H4, H6), 5.26 (s, 2H, H11), 2.87 (s, 4H, H15, H16); ^{13}C NMR (100 MHz, $CDCl_3$, ppm) $\delta = 168.8$ (C14, 17), 165.69 (C12), 143.36 (C1a, 9b), 127.69 (C1, 9), 127.11 (C2, 8), 123.63 (C4a, 6b), 123.54 (C3, 7), 114.8 (C4, 6), 48.78 (C11), 25.63 (C15, 16); FT-IR (KBr, cm^{-1}): 3060 (ν_{CH} aromatic), 2993–2943 (ν_{CH} aliphatic), 1817 ($\nu_{C=O}$ succinimide), 1773–1730 ($\nu_{C=O}$ ester), 1590–1568 ($\nu_{C=C}$), 1204 (ν_{C-O} ester).

N-(methoxy poly(ethylene glycol))-2-(10*H*-phenothiazin-10-yl) acetamide (PPN) was prepared by the amidation reaction of the activated ester [33].



In a 30 mL flask, 0.5 g of **PAcOS** (1 eq) was dissolved in 10 mL acetonitrile under magnetic stirring, at room temperature. Then, 1.06 g methoxy poly(ethylene glycol) amine (PEG-NH₂) (1 eq) and 0.2 mL triethylamine (TEA) (2.2 eq) was added. The reaction mixture was magnetically stirred for 24 h, at the room temperature. The reaction progress has been monitored by TLC. When the reaction was over, the mixture was dried under reduced pressure and the crude product was purified by column chromatography (eluent: DCM/methanol in 10/1, v/v) to give a slightly orange viscous liquid which transformed into a wax when stored into freezer. $\eta = 51$; 1H NMR (400 MHz, $DMSO-d_6$, ppm) $\delta = 8.29-8.26$ (t, 1H, H13), 7.14–7.08 (m, 4H, H1, H2, H8, H9), 6.94–6.90 (t, 2H, H3, H7), 6.72–6.70 (d, 2H, H4, H6), 4.42 (s, 2H, H11), 3.52–3.51 (m, 76H, H13, H14), 3.24 (s, 3H, H15); ^{13}C NMR (100 MHz, $CDCl_3$, ppm) $\delta = 168.37$ (C12), 144.36 (C1a, 9b), 127.66 (C1, 9), 127.43 (C2, 8), 124.73 (C4a, 6b), 123.55 (C3, 7), 115.07 (C4, 6), 70.56 (C15,16), 69.60 (C14), 59.03(C17), 52.22 (C11), 39.11 (C13); FT-IR (KBr, cm^{-1}): 3325 (ν_{NH}), 3060 (ν_{CH} aromatic), 2919–2880 (ν_{CH} aliphatic), 1690 ($\nu_{C=O}$), 1460 (δ_{CH_2} methylene), 1250 (δ_{C-N}), 1106 (ν_{C-O-C}).

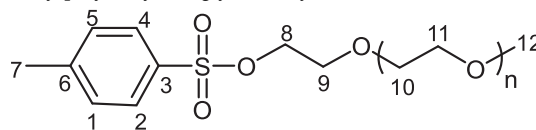
Methoxy poly(ethylene glycol) 2-(10*H*-phenothiazin-10-yl) acetate (PPO) was synthesized by an esterification reaction [34].



In a 10 mL flask cooled at 0 °C, were sequentially introduced, under

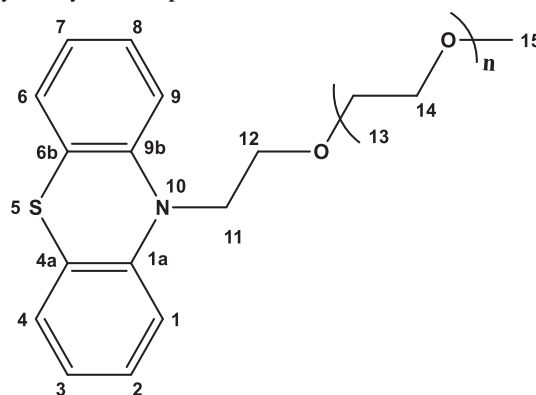
stirring, 0.1 g of **PAcOH** (1 eq), 3 mL DCM, 0.012 g DMAP (0.25 eq) and 0.428 g methoxy poly(ethylene glycol) (2 eq). After 15 min, 0.1 g of *N*, *N'*-dicyclohexylcarbodiimide (DCC) (1.25 eq) was added, and the reaction mixture was maintained for 20 min at 0 °C, and then for 24 h at room temperature. The reaction progress has been monitored by TLC. When the reaction was over, the mixture was filtered, dried under vacuum, re-dissolved in DCM, filtered, and then washed with 100 mL HCl 0.5 M. The organic phase was extracted 3 times with DCM and concentrated by rotary evaporation. The crude product was further purified by column chromatography (DCM/methanol, 10/1, v/v) when an orange viscous liquid was obtained. $\eta = 43\%$; 1H NMR (400 MHz, $CDCl_3$, ppm) $\delta = 7.10-7.07$ (m, 4H, H1, H2, H8, H9), 6.92–6.89 (t, 2H, H3, H7), 6.62–6.60 (d, 2H, H4, H6), 4.55 (s, 2H, H11), 4.42–4.40 (t, 2H, H13), 3.74–3.71 (t, 2H, H14), 3.65–3.60 (m, 30H, H15, H16), 3.37 (s, 3H, H17); ^{13}C NMR (100 MHz, $CDCl_3$, ppm) $\delta = 169.83$ (C12), 144.05 (C1a, 9b), 127.00 (C1, 9), 127.00 (C2, 8), 123.00 (C4a, 6b), 123.07 (C3, 7), 114.59 (C4, 6), 70.5 (C14–16), 64.39 (C13), 59.00 (C17), 50.83 (C11); FT-IR (KBr, cm^{-1}): 3097–3063 (ν_{CH} aromatic), 2904 (ν_{CH_3}), 2875 (ν_{CH_2}), 1742 ($\nu_{C=O}$), 1592–1560 ($\nu_{C=Car}$), 1467 (δ_{CH_2}) 1193 (ν_{C-O-C}), 1109 (ν_{C-O-C}).

Synthesis of 2-methoxy poly(ethylene glycol) 4-methylbenzenesulfonate (Ts-PEG) by poly(ethylene glycol) tosylation [35].



In a Schlenk tube immersed into an ice bath, 0.5 g methoxy poly(ethylene glycol) (1 eq) was dissolved in 1 mL DCM and allowed 5 min to reach 0 °C. Then, 0.04 mL pyridine (Py) (2 eq) and 0.061 g 4-dimethylaminopyridine (DMAP) (2 eq) were added, and the mixture was maintained under stirring for 30 min to obtain a non-protonated reaction intermediate. Further, a solution of 0.0712 g *p*-toluenesulfonyl chloride (Ts) (1.5 eq) dissolved in 1 mL DCM was slowly dropwise during 25 min, and the reaction mixture was allowed to reach room temperature and maintained under vigorous stirring overnight. Finally, the reaction mixture was dissolved in 150 mL DCM and washed with 100 mL HCl 0.5 N. The organic phase was extracted 5 times with 50 mL DCM, and dried under vacuum to give a viscous slightly yellow liquid which was further used without purification. $\eta = 92\%$; 1H NMR (400 MHz, $DMSO-d_6$, ppm) $\delta = 7.22-7.13$ (t and d superposed, 4H, H1, H2, H8, H9), 7.06–7.04 (d, 2H, H4, H6), 6.96–6.92 (t, 2H, H3, H7), 4.06–4.03 (t, 2H, H11), 3.76–3.73 (t, 2H, H12), 3.47–3.42 (m, 48H, H13, H14), 3.24 (t, 3H, H15); ^{13}C NMR (100 MHz, $CDCl_3$, ppm) $\delta = 144.8$ (C6), 132.75 (C3), 129.83 (C1, 5), 127.96 (C2, 4), 70.54–71.90 (C10, 11), 69.25 (C8), 68.64 (C9), 59.01 (C12), 21.63 (C7); FT-IR (KBr, cm^{-1}): 3065 (ν_{CH} aromatic), 2875 (ν_{CH} aliphatic), 1727 ($\nu_{C=O}$), 1693, 1596 ($\nu_{C=C}$), 1465 (δ_{CH_2} methylene), 1350 ($\nu_{S=O}$ sulfone), 1108 (ν_{C-O-C}).

Synthesis of 10-(methoxy poly(ethylene glycol))-10*H*-phenothiazine (PP) by *N*-alkylation of phenothiazine [12].



In a round bottom three necked flask immersed into an ice bath, 0.065 g NaH (2.2 eq) was dissolved in 7 mL DMF, under nitrogen atmosphere and allowed to reach 0 °C (20 min). Then, a solution of 0.2565 g phenothiazine (1 eq) in 3 mL DMF was added through a septum. After 20 min, when the mixture got an intense orange colour, a solution of 0.95 g Ts-PEG (1 eq) in 3 mL DMF was slowly dropwise during 30 min. After that, the reaction mixture was allowed to reach room temperature and kept under vigorous magnetic stirring for 24 h. The reaction progress was monitored by TLC. When the reaction was finished, the mixture was washed with brine and filtered to remove precipitated impurities. The organic phase was extracted 3 times with DCM, dried with MgSO₄, filtered, and then concentrated by rotary evaporation. The crude product was purified by column chromatography (DCM:methanol 10:1, v/v) to give a deep red viscous liquid. $\eta = 37\%$; ¹H NMR (400 MHz, DMSO-*d*₆, ppm) $\delta = 7.22\text{--}7.13$ (t,d, 4H, H1, H2, H8, H9), 7.06–7.04 (d, 2H, H4, H6), 6.97–6.93 (t, 2H, H3, H7), 4.07–4.04 (t, 2H, H11), 3.76–3.73 (t, 2H, H12), 3.50–3.42 (m, 48H, H13, H14), 3.24 (t, 3H, H15); ¹³C NMR (100 MHz, DMSO-*d*₆, ppm) $\delta = 145.02$ (C1a,9b), 128.12 (C1, 9), 127.55 (C2,8), 123.76 (C4a, 6b), 123.07 (C4, 6), 116.15 (C3, 7), 70.24 (C13,14), 67.93 (C12), 58.51(C15), 47.52 (C11); FT-IR (KBr, cm⁻¹): 3060 (ν CH aromatic), 2870 (ν CH aliphatic), 1593, 1570 (ν C=C), 1460 (δ CH₂), 1292 (ν C-N), 1110 (ν C-O-C), 755 (δ C-H).

2.3. Aggregate formation

Stock solutions were prepared by dissolving 0.2 mol of compounds in 2 mL ultrapure water to give 100 mM solutions. Serial dilutions were then realized by slowly dropping 1 mL of solution of superior concentration in 9 mL water, under vigorous magnetic stirring, for 10 min (e.g. 1 mL solution 100 mM was dissolved in 9 mL ultrapure water to give a solution of 10 mM, and so on). For ageing investigation, the solutions were stored at 25 °C, and magnetically stirred for 10 min before measurements.

For AFM and microscopy under UV light, the solutions of 1 mM of the compounds were casted on glass lamella and fast dried under an UV lamp.

For POM and SEM measurements, the PP compound was embedded in solid polyvinyl borate (PVAB) matrix by microemulsion method, when a PP solution in water was dispersed in a 7% PVAB water solution to obtain three different concentrations [36]. Thus 100 μ L of 100 mM PP solution was dispersed in 900 μ L PVAB solution to obtain 10 mM PP in PVAB; 100 μ L of 10 mM PP solution was dispersed in 900 μ L PVAB solutions to obtain 1 mM PP in PVAB; and 100 μ L of 1 mM PP solution was dispersed in 900 μ L PVAB 1 to obtain 10⁻¹ mM PP in PVAB. 300 μ L of each concentration were poured on glass lamella and dried in an oven under reduced pressure at 50 °C.

2.4. Equipment and methods

Infrared spectra were recorded on a FTIR Bruker Vertex 70 Spectrometer, in the transmission mode, using KBr pellets, at room temperature, with a resolution of 2 cm⁻¹ and accumulation of 32 scans. The spectra were processed using Origin8 software.

NMR spectra were obtained on a Bruker Avance DRX 400 MHz spectrometer equipped with a 5 mm QNP direct detection probe and z-gradients, at room temperature, with an accumulation of 64 scans. The chemical shifts were reported as δ values (ppm) relative to the residual peak of the solvent.

UV-Vis absorption and photoluminescence spectra were recorded on a Carl Zeiss Jena SPECORD M42 spectrophotometer and a PerkinElmer LS 55 spectrophotometer, respectively, in water solutions, from 10 mM up to 10⁻⁶ mM, using 1 cm quartz cells. The energy band gap (E_g) was estimated from the equation: $E_g = h \times c / \lambda_{\max} = 1240.8 / \lambda_{\max}$, where h is the Planck constant, c is the light velocity, and λ_{\max} is the wavelength of the absorption maximum, in the optical absorption

spectra.

Hydrodynamic diameter and distribution of the particles was measured using Delsa Nano C, Beckman Coulter equipment on water solutions, with concentration from 10 mM up to 10⁻¹ mM, using 1 cm glass cells, at room temperature (25 °C). The scattering light was measured at the fixed angle of 165°, pinhole 50 μ m, refractive index 1.3328 (water), viscosity (cP) 0.8878, dielectric constant 77.3. The measurements were done on fresh solutions and after an ageing period of one week and eight weeks, in order to assess the particle stability.

SEM images were acquired with a Scanning Electron Microscope SEM EDAX – Quanta 200) at lower accelerated electron energy of 20 Kev, on PP sample embedded into a solid matrix (see the preparation of the aggregates).

Atomic force microscopy was performed on a Solver PRO-M, NT-MDT, Russia instrument, in semi contact mode. Nova v.1443 software was used for recording and analysing the AFM topographic and phase contrast images. The samples were prepared by casting the solutions of different concentrations on glass lamella.

To investigate the ordered nature of the particles, the samples were observed with an Olympus BH-2 polarized light microscope on the PP sample embedded into a solid matrix (see preparation of the aggregates).

Optical micrographs under UV light were obtained with a Nikon Eclipse TE2000-U microscope equipped with a fluorescence illuminator with a 450–490 nm (pyronine) band – pass excitation filter. The samples were prepared by casting solutions on a glass lamella and fast drying under an UV lamp.

2.5. Cell cultures

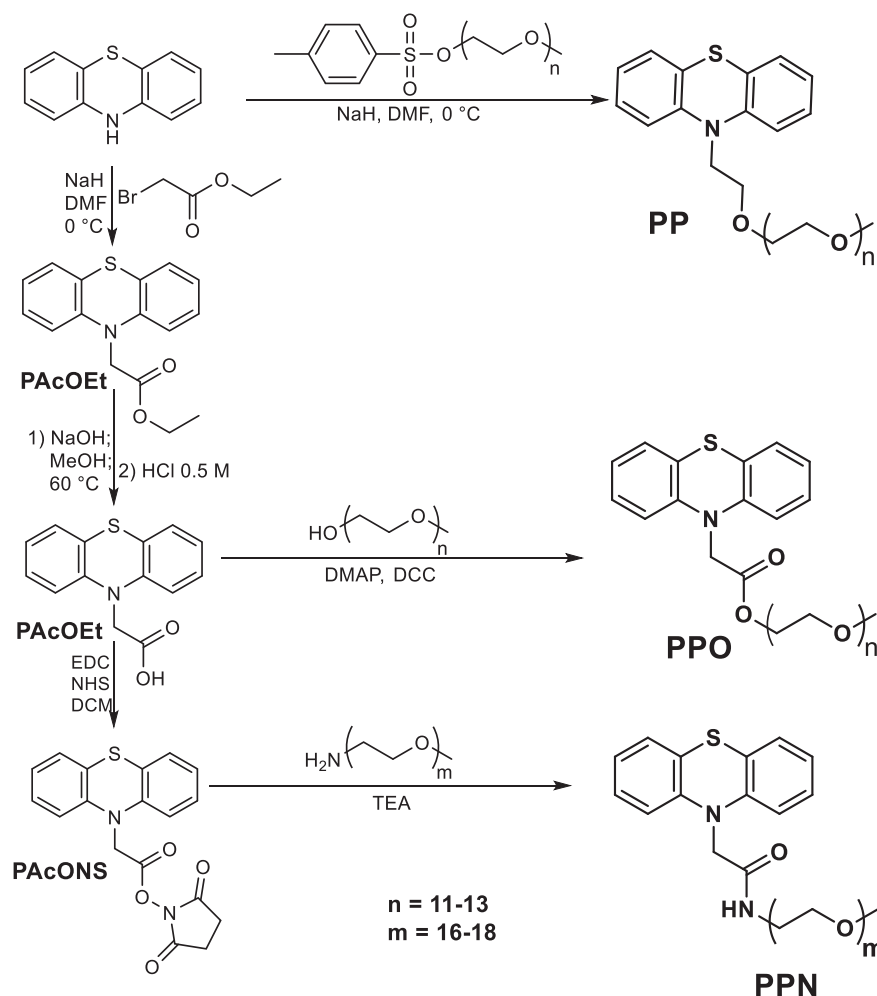
NHDF cells (normal human dermal fibroblasts cells from PromoCell) and HeLa cells (human cervical cancer cells from CLS-Cell-Lines-Services-GmbH, Germany) were cultivated in tissue culture flasks with alpha-MEM medium (Lonza) supplemented with 10% fetal bovine serum (FBS, Sigma Aldrich) and 1% Penicillin-Streptomycin-Amphotericin B mixture (10 K/10 K/25 μ g in 100 mL, Lonza). Medium was changed with a fresh one each 3 days. Once cells reached confluency, they were detached with 1 \times TrypLE™ Express Enzyme (Gibco), washed with phosphate buffered saline (PBS, Invitrogen), centrifuged at 200 \times for 3 min and sub-cultured into 96-well plates.

2.6. In vitro cytotoxicity study

Cytotoxicity of the studied compounds was measured using the CellTiter 96® Aqueous One Solution Cell Proliferation Assay (Promega), a metabolic assay (MTS) which measures the mitochondrial reductase activity in cells. The cytotoxicity was evaluated in water solutions, in a range of concentrations starting from 10 mM to 10⁻⁶ mM. Medium was used in the control wells. HeLa cells were seeded at a density of 1 \times 10⁴ cells per well and NHDF cells were seeded at a density of 5 \times 10³ in 100 μ L culture medium (alpha-MEM medium supplemented with 10% v/v fetal bovine serum (FBS) and 1% v/v Penicillin-Streptomycin-Amphotericin B mixture (10 K/10 K/25 μ g) in 96 well cell culture plates. After 24 h, the medium in each well was replaced with 100 μ L mixture containing fresh medium and the studied solution. After 45 h, 20 μ L of CellTiter 96® Aqueous One Solution reagent were added to each well, and the plates were incubated for another 3 h before reading the result. Absorbance at 490 nm was recorded with a plate reader (iMark, Bio-Rad). Cell viability was calculated and expressed as percentage relative to the viability of untreated cells \pm SEM (standard error of the mean), $n = 5$.

2.7. Statistical analysis

Two way ANOVA using Tukey's multiple comparisons test was performed in GraphPad Prism7 for Windows (GraphPad Software, San



Scheme 1. Synthesis of the PEGylated derivatives.

Diego, CA) to determine the differences between groups. The differences are statistically significant when $P < 0.05$.

3. Results and discussions

3.1. Synthesis

A series of three PEGylated phenothiazine derivatives were synthesized by grafting PEG chains to the nitrogen atom of phenothiazine, via three different connecting units. The connection of PEG to phenothiazine by an ether unit was realized by N-alkylation reaction with a prior synthesized tosylate PEG derivative (coded **PP**). The PEGylated phenothiazine including an amide unit (coded **PPN**) was prepared by a reaction chain via a phenothiazine activated ester intermediate, while the PEGylated phenothiazine containing an ester unit (coded **PPO**) was prepared by an esterification reaction of the phenothiazine acetic acid intermediate. Their synthesis was represented in the Scheme 1.

The successful synthesis of the targeted **PP**, **PPO** and **PPN** compounds was confirmed by FTIR and NMR spectroscopies. FTIR spectra displayed characteristic vibrations of the phenothiazine ring and PEG chains for the three compounds, and specific vibrations bands of amide and ester linking groups for **PPN** and **PPO**, respectively (Fig. 1). Thus, the amide C=O stretch was noted at 1690 cm^{-1} , while the ester C=O stretch occurred at 1742 cm^{-1} [15,33].

In the ^1H NMR spectra was noted the disappearance of the chemical shift characteristic for the proton linked to the nitrogen atom of phenothiazine, and the presence of the chemical shifts of the aromatic and

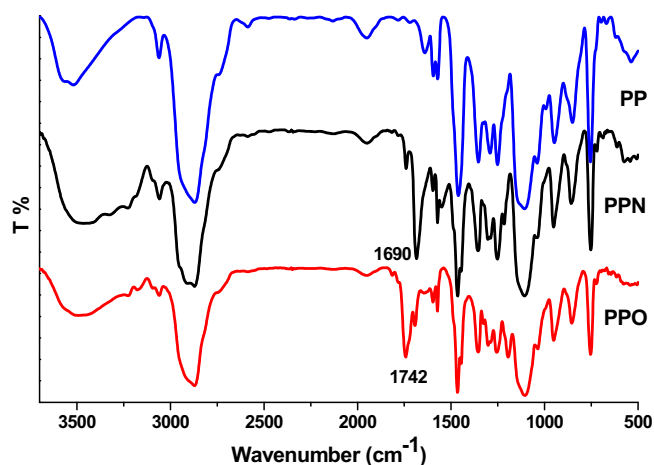


Fig. 1. FTIR spectra of the PEGylated phenothiazine derivatives.

aliphatic protons in the right ratio of the integrals. In the case of **PPN** derivative, the chemical shift of the amide proton occurred at 8.39–8.26 ppm (Figs. 2, S1) [33]. Moreover, ^{13}C NMR spectra evidenced the chemical shift of all carbon atoms (Fig. S1). All these spectral data indubitable confirmed the right structure of the **PP**, **PPO** and **PPN** compounds and their high purity.

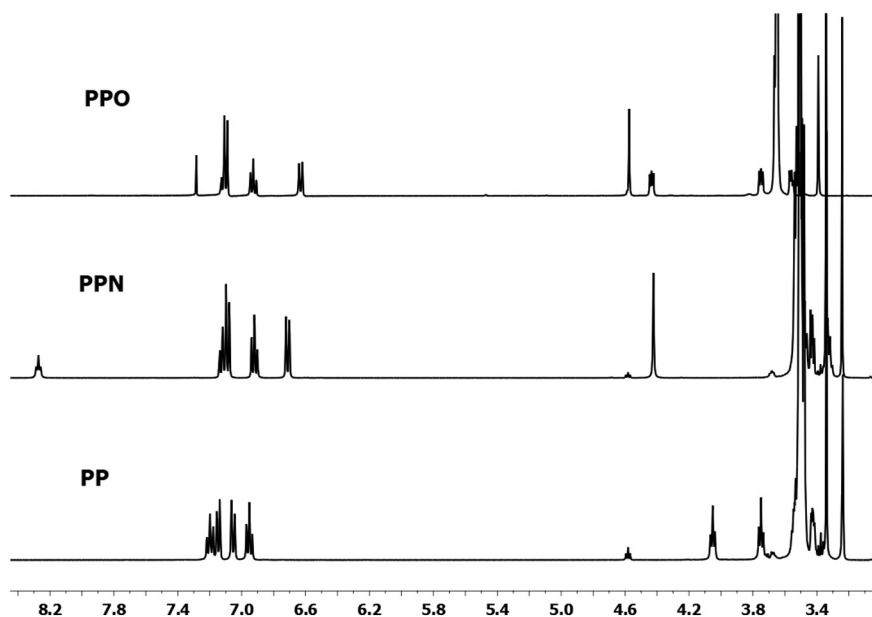


Fig. 2. ^1H NMR spectra of the PEGylated derivatives.

3.2. Water solubility and hydrolytic stability

The three PEGylated derivatives were viscous liquids, completely soluble in water and common organic solvents, such as methanol, ethanol, acetone, THF, DMF, for concentrations lower than 100 mM. Their water solutions were macroscopic clear over 5 days of observation. On day 5, a slight turbidity was noticed for the water solution of PPO (100 mM), correlated with the self-ordering of the molecules in supramolecular architectures.

The aim of the paper was the synthesis of phenothiazine derivatives intended for further use as building blocks for bio-materials. In this sense, an important aspect is their hydrolytic stability, being known that ester linking group may have a reversibility degree in aqueous environment [37]. To investigate it, the samples were dissolved in deuterium oxide and their ^1H NMR spectra were recorded at different moments over 7 days (Fig. S2). No differences were discriminated between them, the chemical shifts and their integrals were maintained at the same values and no additional chemical shifts appeared. This was a good indicator that no degradation products appeared, and the samples were hydrolytically stable.

3.3. Photophysical investigation

The samples formed coloured macroscopically clear solutions with strong luminescence under an UV lamp, when dissolved in any solvent. The luminescence colour and intensity varied with the sample structure and solvent polarity (Fig. 4). As PEG is well known as a non-ionic amphiphilic agent who favours the self-assembling, this optical behaviour was assigned to the formation of aggregates by a hydrophobic phenothiazine –hydrophilic PEG segregation [19]. Being known that photophysical behaviour is sensitive to the formation of aggregates [19,38,39], the ability of the synthesized compounds to self-assemble was investigated by UV–vis and photoluminescence spectroscopy, on solutions prepared by serial dilution in water, from 10 to 10^{-6} mM. For an accurate interpretation of the data, the spectra were recorded on the pristine phenothiazine (PTZ) solution as well.

A comparative analysis of the UV–vis spectra revealed common features indicating similar aggregation behaviour, as follows (Figs. 3, S3). Pristine phenothiazine solution showed a sharp absorption band with maximum at 250 nm and a broader band of lower intensity around 279 nm, characteristic to the $\pi\text{-}\pi^*$ and $n\text{-}\pi^*$ electronic transitions

[17,40]. The absorption edge laid at 370 nm. For all three studied compounds (PP, PPO, PPN), the solutions of 10^{-1} , 10^{-2} and 10^{-3} mM preserved the PTZ absorption profile, but the absorption band of lower energy (279 nm) was bathochromic shifted about 25 nm, to 303–306 nm, phenomenon characteristic to the occurrence of sub-micrometric particles [19,41]. This indicated the segregation of the phenothiazine units *via* intermolecular forces which favoured the electron delocalization along the phenothiazine, and consequently the decrease of HOMO-LUMO band gap (Table 1). Besides the bathochromic shift, a decrease of the adsorption width of the half maximum (FWHM) could be observed for the compounds solutions too (Table 1). This adsorption behaviour is characteristic to a head-to-tail arrangement of a J-type coupling, in concordance with the segregation of the phenothiazine heteroaromatic rings into the central part forming a hydrophobic core and PEG at the edge [42,43]. For the most concentrated solutions, 10 and 1 mM, a new absorption band in the visible domain appeared (512, 562 nm, respectively), indicating a possible more extent conjugation of the phenothiazine core. This should be correlated with the excimer formation under the pressure of the high concentration which favours the formation of aggregates of high density [44]. In such a way, the high density of PEG units wrapping the phenothiazine ones confines the phenothiazine hydrophobic core. For the most diluted samples (10^{-4} - 10^{-6} mM) the absorption profile displayed only a broad band of low intensity. It can be appreciated that for concentrations lower than 10^{-4} mM, no stable aggregates were wet formed. A graphical representation of the absorbance *versus* concentration indicated two linear sections with different slopes with the intercept corresponding to the critical aggregation concentration around 8×10^{-4} mM: 7.06×10^{-4} , 8.7×10^{-4} and 9.47×10^{-4} mM for PPN, PP and PPO respectively (Fig. S4) [45]. However, the PPO compound with ester connection, showed bathochromic shifted UV–vis absorption bands of low intensity even for concentrations lower than 10^{-4} mM (Fig. S3). A distinct behaviour of PPO compared to the other compounds was also observed for the photophysical parameters: the lowest energy band-gap (4.05 compared to 4.08 and 4.09), the lowest FWHM (52 compared to 66.4 and 67) and the most hypsochromic shifted absorption edge (369 compared to 410 and 392 nm). Considering also the DLS data, the distinct behaviour of PPO can be correlated with its ability to self-assemble into smaller J-type aggregates at lower concentrations [42,43].

Further, the luminescence behaviour of the samples was

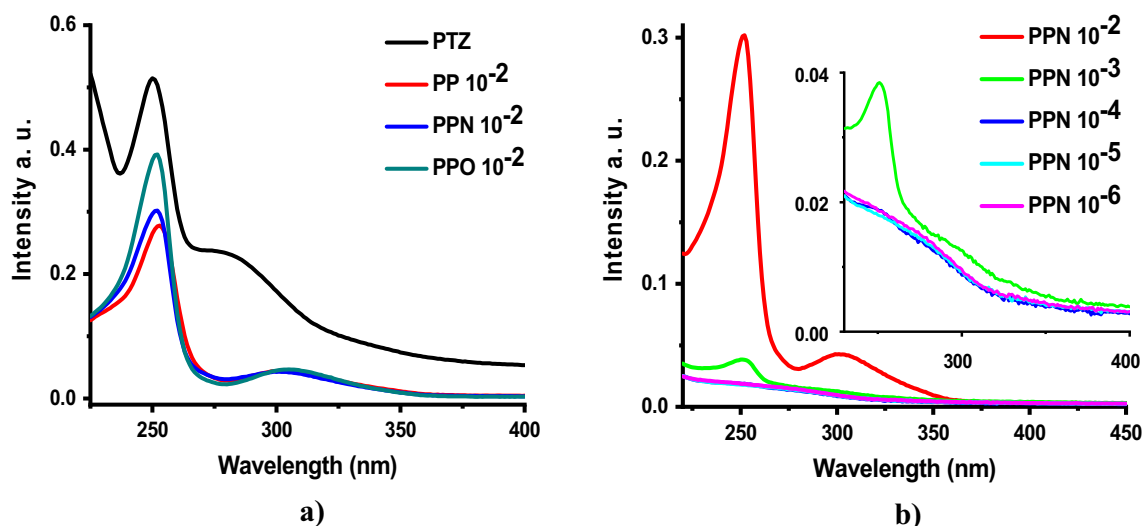


Fig. 3. Representative absorption spectra of the water solutions of the a) compounds (10^{-2} mM) and b) PPN (10^{-2} - 10^{-6} mM). The concentrations were given in the legend along the codes. The inset represents the magnification of the spectral domain from 200 to 400 nm.

Table 1

Absorption parameters of the studied compounds in water (10^{-2} mM).

Code	PTZ	PP	PPN	PPO
λ_{\max} (nm)	279	304	303	306
E_g (eV)	4.48	4.08	4.09	4.05
FWHM (nm)	87.2	66.4	67	52
λ_{edge} (nm)	403	410	392	369
Stocks shift (nm)	–	144	140	137

λ_{\max} : absorption maximum; E_g : the optical band-gap calculated for absorption maximum; FWHM: the full-width-at-half-maxima; λ_{edge} adsorption edge.

investigated by exciting the solutions with light of wavelength corresponding to the absorption maxima (Figs. 4, S5). The emission spectra presented a similar pattern for the three compounds, with an emission band in the blue region. The most intense blue emission was recorded when the solutions of 10^{-1} mM were excited with light wavelength corresponding to the absorption of the conjugated system tuned by the aggregates formation (around 305 nm) (Fig. S5). The intensity drastically diminished when the concentration decreased, about 7 times lower for the 10^{-2} mM, and to insignificant values for the others (Figs. 4b, S5). The most intense luminescence was recorded for the PP samples (Figs. 4a, S5). The lower intensity of the most concentrated samples (10, 1 mM) was correlated with the luminescence quenching

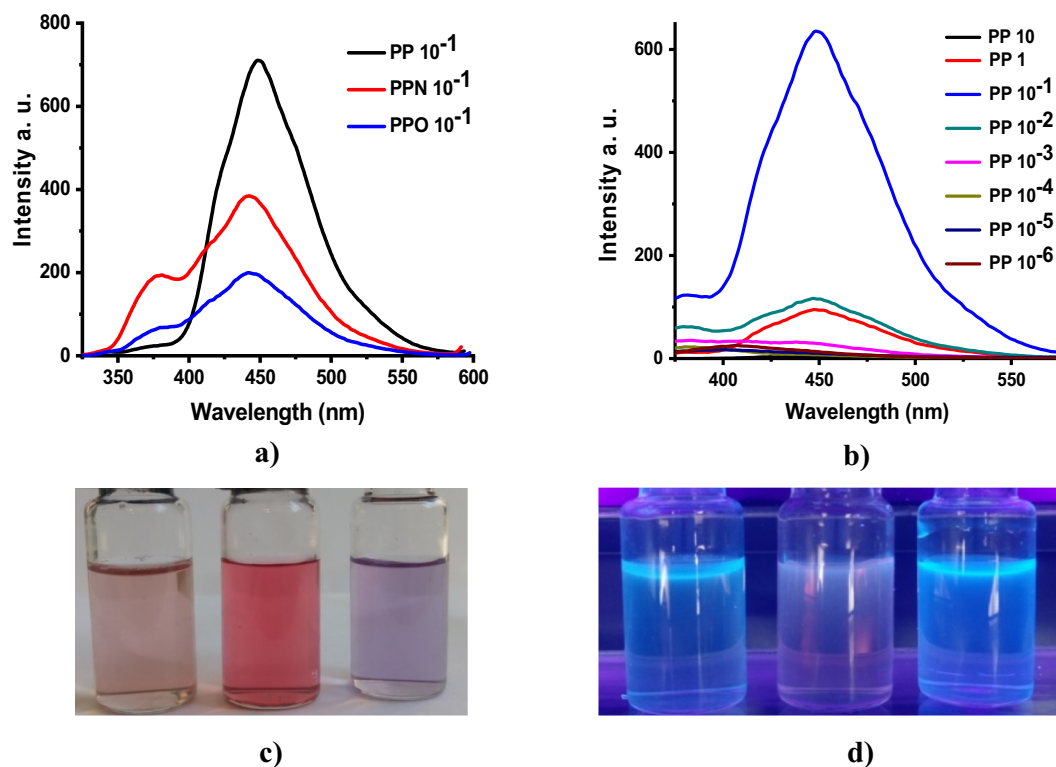


Fig. 4. Representative emission spectra of the water solutions of the a) compounds (10^{-1} mM) and b) PP of different concentrations, when excited with light around 305 nm. Images of the water solutions under c) daily light and d) UV-lamp, from left to right: PPO, PPN, PP.

due to the stronger intermolecular forces, while in the case of the samples of lower concentration ($<10^{-3}$ mM) was correlated with the low amount of fluorophore units [19]. It should be remarked that PPO, compared to PP and PPN, displayed emission bands even for concentrations of 10^{-3} and 10^{-4} mM. This correlated well with the ability of PPO to form aggregates of lower dimensions compared to PP and PPN, leading to a higher number of fluorophores (see Section 3.4. Investigation of the self-assembling behaviour). Unexpected, when excited with light of higher energy ($\lambda \cong 250$ nm), the blue emission intensity decreased, and an inversion on the scale of the emission intensity was noted for 10^{-2} mM and 10^{-1} mM solutions, i.e. the emission intensity of the 10^{-2} mM solutions was higher than 10^{-1} mM ones (Fig. S5). This was correlated with the strength of the intermolecular forces – luminescence quenching relationship [46]. Exciting with light corresponding to the wavelength of UV lamp (365 nm), the luminescence intensity significantly decreased in accordance with the too low energy compared to the molecule's band gap (Fig. S5). In this case, the most intense emission was given by the most concentrated samples (10 and 1 mM), in agreement with a better fitting with the lower band gap triggered by the stronger intermolecular forces. For these two concentrations, an emission of yellow light was also observed when excited with light of even lower energy, corresponding to their absorption at 512–562 nm (Fig. S5).

The alteration of the emission intensity when the concentration changed suggests a close correlation with the parameters defining the aggregates (such as diameter and polydispersity), the possible connection being the strength of the intermolecular forces developed among the phenothiazine heterocycles under the pressure of self-assembling. Considering that the synthesized molecules have no fluorophore units, the luminescence was attributed to an aggregation induced emission phenomenon, triggered by the self-assembling of the hydrophobic-hydrophilic PEGylated phenothiazines [47,48]. Interesting for further bio-applications is the possibility to selectively tune the luminescence, by triggers as solution concentration and the energy of the exciting light.

3.4. Investigation of the self-assembling behaviour

There are some peculiarities which characterize the aggregate formation: the shape and hydrodynamic diameter – which should be proved by DLS, AFM, and SEM measurements, the hydrophobic-hydrophilic ordering – which should be proved by a birefringent appearance under polarized light, and light emission which should be seen when exciting with UV light. To evidence them, dynamic light scattering, atomic force microscopy, UV-light microscopy and polarized light microscopy were recorded on water solutions (DLS) or solid samples prepared by casting the water solutions on thin glass lamella and fast drying under an UV lamp (AFM, UV-light microscopy), or by dispersing into a solid polymer matrix (POM, SEM).

DLS certainly confirmed the formation of submicrometric aggregates in water, with a major population with average hydrodynamic diameter less than 322 nm, for concentrations comprised in the range 10^{-1} – 10^{-3} mM (Figs. 5a, S6). As a general rule, the diameter decreased as the concentration decreased. Thus, for PP fresh samples, the diameter decreased from 289 to 106 nm. Over time, the diameter progressively increased, reaching values close to 800 nm in two months, in agreement with a continuous aggregation of the aggregates. PPN revealed a less accentuated variation of the hydrodynamic diameter, which decreased from 264 to 176 nm for fresh samples, and showed insignificant variations over time (Fig. S6). This excellent stability can be correlated with the presence of the amide linker which prompted strong H-bonds and the higher length of the PEG chain leading to a higher surface density, less susceptible to dissolution [29,49]. Interesting, in the case of PPO, the diameter drastically decreased as the concentration decreased, from 322 to 63 nm. The aggregates were less stable, their diameter reaching almost double size over 6 days. It appears that the stronger H-bonds developed among the amide groups favoured the

formation of stable aggregates over time, while the less strong H-bonds developed among the ester groups contributed for the formation of aggregates of lower dimension at lower concentrations in the case of PPO compound [29,30,50].

The aggregation tendency was further confirmed by AFM and SEM microscopy (Figs. 6a, b, c, S7). Despite some size alterations driven by the preparation of the solid samples, i.e. dehydration and coalescence processes with antagonistic effect on the diameter, AFM and SEM images revealed aggregates of spherical shapes (Figs. 6a, b, c, S7). UV light microscopy provided images of the round shapes emitting blue light when excited in the blue region, confirming the correct attribution of the luminescence to the aggregate formation (Fig. 6d, e, f). The images acquired under polarized light displayed birefringent droplets confirming the hydrophobic/hydrophilic self-assembling as the main driving force of the aggregate formation (Fig. 6g, h, i). All these data allow concluding that the PEGylated phenothiazines have the ability to self-assemble in submicrometric aggregates, property which can be explored for the preparation of drug delivery systems for release of poorly water soluble compounds [51,52].

3.5. In vitro biocompatibility

The new compounds were designed having in mind their use as building blocks for bio-applications. To this end, their biocompatibility was investigated *in vitro* on normal human dermal fibroblasts (NHDF) as model for normal cells. Bearing in mind the antitumor promoting effect of some phenothiazine based compounds, the activity on human cervical cancer cells (HeLa) as model tumor cells, was examined too. The measurements were done on eight solution samples of different concentrations, from 10 to 10^{-6} mM, for each compound, in order to establish the concentration - biocompatibility relationship (Fig. 7). All samples showed NHDF viability higher than 80% for concentrations lower than 10^{-1} mM. Higher cell viability could be remarked for the concentration range 10^{-5} – 10^{-1} mM, the most probably associated with the aggregate formation. The lower concentration compared to the critical aggregation concentration can be attributed with the increased rate of self-assembling in the medium of higher ionic strength [53,54]. It can be envisaged that coverage of the phenothiazine with biocompatible PEG into aggregates, is an effective method to improve the phenothiazine biocompatibility [55]. Among the PEGylated phenothiazines, a better cell viability was recorded for PPN. This can be correlated with the highest stability of its aggregates. It is also possible as the presence of the amide linking group, a chemical component of proteins in cells, to bring a plus for the biocompatibility improvement [31,50].

An interesting behaviour was noted when the compounds were in contact with HeLa cells. For concentrations in the range 10^{-5} – 10^{-2} mM, the cell viability was higher than 90%, with no obvious cytotoxic effect. Nevertheless, for the concentration of 10^{-1} mM, the presence of the ester linkage inflicted a dramatic cytotoxicity, the HeLa cell viability diminishing at 34% compared to 58% for PP and 90% for PPN. This result was confirmed when the tests were repeated three times, at different moments. It is worthy to remark that the utmost antitumor behaviour was recorded for the smallest aggregates revealed by DLS, i.e. PPO gave aggregates with average hydrodynamic diameter of 63 nm at 10^{-1} mM. It should be noted that PP, which showed less strong antitumor activity at 10^{-1} mM, revealed by DLS aggregates of higher dimension, i.e. 248 nm. Another important aspect is related to the aggregate stability. PPN which displayed the most stable aggregates didn't showed obvious cytotoxicity against HeLa cells. It is possible that the small dimension combined with the less stability of the PPO aggregates to play an important role in the delivery of the PPO molecules to the undifferentiated tumor cells [56]. This hypothesis is supported by literature data which indicate that an optimal size of the nanoparticles for anticancer activity lays around 50 nm, value close to that of 63 nm recorded by DLS for PPO 10^{-1} mM [57]. Moreover, a literature survey

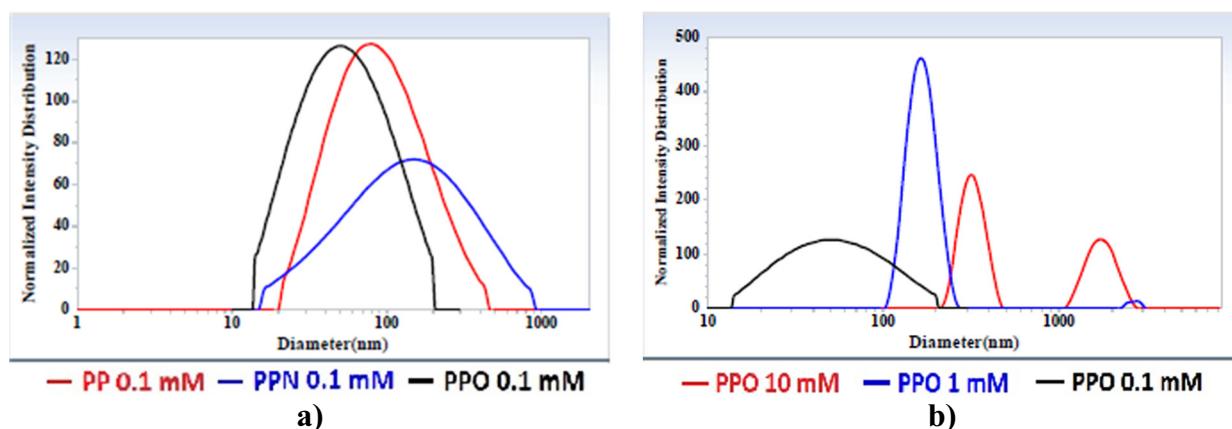


Fig. 5. DLS graphs of the a) studied compounds and b) PPN over two month ageing, in water solutions. The codes along with concentrations were given under the graph).

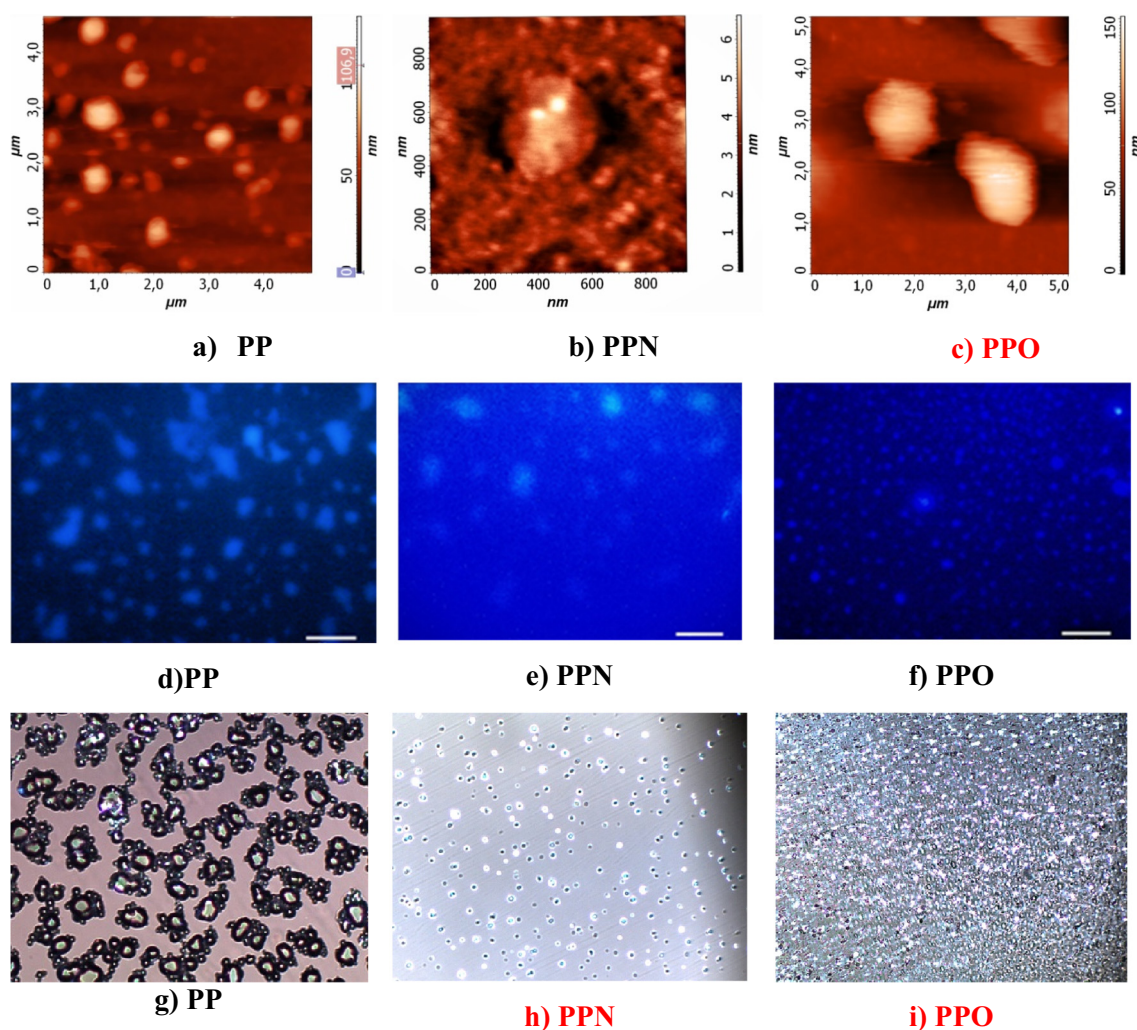


Fig. 6. Representative a, b, c) AFM, d, e, f) POM and g, h, i) UV light microscopy images of the studied compounds. POM magnification: $400\times$. AFM scale bar: 20 μm .

reveal that ester linkage seem to play an important role for antitumor activity. We found that ester based prodrugs of camptothecin demonstrated superior antitumor activity compared to the pristine camptothecin, but not a clear structure-antitumor activity was evidenced [58]. In the same line of thought, a large variety of esters of natural originating acids, such as caffeic acid [59], α -lipoic acid [60], betulinic acid [61], cinnamic acid [62] proved improved anticancer activity

compared to their precursors while having excellent biocompatibility, but the mechanism of their action is yet to be elucidated. Some protein farnesyltransferase inhibitors demonstrated improved antitumor activity when their structure comprised a chemical stable ester unit, being envisaged its possible involving in the growth inhibition of the tumor cells [63]. Further browsing the literature, it should be stressed that amide-to-ester mutations are possible and they can serve as triggers of

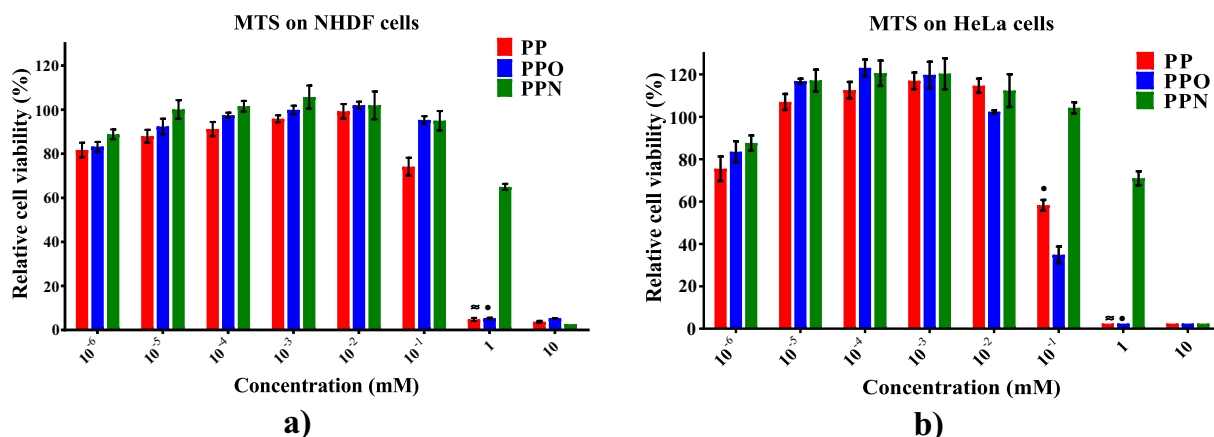


Fig. 7. Cell viability on a) normal human dermal fibroblasts (NHDF) and b) human cervical cancer cells (HeLa). Values are expressed as mean cell viability \pm SEM, n = 5. Reduction of cell viability by more than 30% is considered a cytotoxic effect. * P < 0.05 for PPO vs PPN, \approx P < 0.05 for PP vs PPN by 2way ANOVA using Tukey's multiple comparisons test.

tumor cells inhibition [64]. All these entitle to believe that the combination of phenothiazine, PEG, and ester units resides in a unique design with antitumor activity, which will be systematically developed and investigated in order to reveal a possible activity mechanism.

4. Conclusions

A series of three new PEGylated phenothiazine derivatives were successfully synthesized by grafting hydrophilic PEG to the nitrogen of hydrophobic phenothiazine, via an ether, ester, or amide linking group. They proved excellent solubility in common solvents and water bi-dispersant, hydrolytic stability, and self-assembling in water to form submicrometric aggregates. The aggregates based a head-to-tail arrangement showed ageing stability correlated with the linking unit. They induced light emission, which could be tuned by the concentration and the energy of the exciting light. *In vivo* biocompatibility tests revealed high biocompatibility on normal human dermal fibroblasts, for concentrations up to 1 mM. The PEGylated phenothiazine containing ester units showed cytotoxicity against human cervical cancer cells at the concentration of 10^{-1} mM. Both, biocompatibility and cytotoxicity, were correlated to the aggregate formation, their size and stability. All these properties indicate the new synthesized compounds as high performance candidates for image guided therapy and drug delivery systems for release of poor water soluble components. Also, they are valuable building blocks for developing anticancer drugs and ecologic optoelectronic materials.

CRedit authorship contribution statement

Sandu Cibotaru: Formal analysis, Investigation, Software, Writing - original draft. **Andreea-Isabela Sandu:** Formal analysis, Investigation, Software. **Dalila Belei:** Conceptualization, Formal analysis, Investigation. **Luminita Marin:** Conceptualization, Data curation, Funding acquisition, Methodology, Project administration, Supervision, Writing - original draft, Writing - review & editing.

Declaration of competing interest

The authors declare that they have no known competing financial interests or personal relationships that could have appeared to influence the work reported in this paper.

Acknowledgements

The paper was supported by a project financed through a Romanian National Authority for Scientific Research MEN – UEFISCDI, grant project PN-III-P4-ID-PCCF-2016-0050 and European Union's Horizon 2020 - Research and Innovation Framework Programme (grant agreement 667387).

Appendix A. Supplementary data

Supplementary data to this article can be found online at <https://doi.org/10.1016/j.msec.2020.111216>.

References

- [1] J. Al-Busaidi, A. Haque, N.K. Al Rasbi, M.S. Khan, Phenothiazine-based derivatives for optoelectronic applications: a review, *Synthetic Met* 257 (2019) 116189.
- [2] B. Varga, Á. Csonka, A. Csonka, J. Molnár, L. Amaral, G. Spengler, Possible biological and clinical applications of phenothiazines, *Anticancer Res.* 37 (11) (2017) 5983–5993.
- [3] A.P. Kulkarni, X. Kong, S.A. Jenekhe, High-performance organic light-emitting diodes based on intramolecular charge-transfer emission from donor-acceptor molecules: significance of electron-donor strength and molecular geometry, *Adv. Funct. Mater.* 16 (2006) 1057–1066.
- [4] K.P. Morak-Mlodawska, M. Jeleń, Recent progress in biological activities of synthesized phenothiazines, *Eur. J. Med. Chem.* 46 (2011) 3179–3189.
- [5] G. Sudeshna, K. Parimal, Multiple non-psychiatric effects of phenothiazines: a review, *Eur. J. Pharmacol.* 648 (2010) 6–14.
- [6] S. Ahmadian, V. Panahi-Azar, M.A.A. Fakhree, W.E. Acree, A. Jouyban, Solubility of phenothiazine in water, ethanol, and propylene glycol at (298.2 to 338.2) K and their binary and ternary mixtures at 298.2 K, 4352–4355, *J. Chem. Eng. Data* 56 (2011) 4352–4355.
- [7] C. Capello, U. Fischer, K. Hungerbühler, What is a green solvent? A comprehensive framework for the environmental assessment of solvents, *Green Chem.* 9 (2007) 927–934.
- [8] C. Satheeshkumar, M. Ravivarma, P. Rajakumar, R. Ashokkumar, D.C. Jeong, C. Song, Synthesis, photophysical and electrochemical properties of stilbenoid dendrimers with phenothiazine surface group, *Tetrahedron Lett.* 56 (2015) 321–326.
- [9] Y. Xie, et al., An aqueous fluorescent sensor for Pb²⁺ based on phenothiazine-polyamide, *Spectrochim. Acta A* 18 (2018) 1386–1425.
- [10] J. Fix, P. Lepperpita, T. Porterjo, S. Lexan, The use of phenothiazines to enhance the rectal absorption, *J. Pharm. Pharmacol.* 36 (1984) 286–288.
- [11] S. Imabayashi, K. Ishii, M. Watanabe, Effect of the modification of phenothiazine-labeled poly(ethylene oxide) on the solubility and enzymatic electrocatalytic reaction of glucose oxidase in water/1-butyl-3-methylimidazolium tetrafluoroborate mixtures, *Electrochem. Commun.* 8 (2006) 45–50.
- [12] D. Soni, N. Duvva, D. Badgurjar, T.R. Kanchan, S. Nimesh, G. Arya, L. Giribabu, R. Chitta, Hypochlorite mediated modulation of photo-induced electron transfer in PTZ-BODIPY electron donor-acceptor dyad: a highly water soluble “turn-on” fluorescent probe for hypochlorite, *Chem. Asian J.* 13 (2018) 1594–1608.
- [13] Z. Long, M. Liu, K. Wang, F. Deng, D. Xu, L. Liu, Y. Wan, X. Zhang, Y. Wei, Facile synthesis of AIE-active amphiphilic polymers: self-assembly and biological imaging applications, *Mat. Sci. Eng. C* 66 (2016) 215–220.

- [14] A. Zabolica, M. Balan, D. Beleu, M. Sava, B.C. Simionescu, L. Marin, Novel luminescent phenothiazine-based Schiff bases with tuned morphology. *Synthesis, structure, photophysical and thermotropic characterization, Dyes Pigments* 96 (2013) 686–698.
- [15] D. Beleu, C. Dumea, E. Bicu, L. Marin, Phenothiazine and pyridine-N-oxide based AIE-active triazoles: synthesis, morphology and photophysical properties, *RSC Adv.* 5 (2015) 8849–8858.
- [16] A. Bejan, S. Shova, M.-D. Damaceanu, B.C. Simionescu, L. Marin, Structure-directed functional properties of phenothiazine brominated dyes: morphology and photo-physical and electrochemical properties, *Cryst. Growth Des.* 16 (2016) 3716–3730.
- [17] L. Marin, A. Bejan, D. Ailincăi, D. Beleu, Poly(azomethine-phenothiazine)s with efficient emission in solid state, *Eur. Polym. J.* 95 (2017) 127–137.
- [18] A. Bejan, D. Ailincăi, B.C. Simionescu, L. Marin, Chitosan hydrogelation with a phenothiazine based aldehyde – toward highly luminescent biomaterials, *Polym. Chem-UK.* 9 (2018) 2359–2369.
- [19] A. Bejan, L. Marin, Phenothiazine based nanocrystals with enhanced solid state emission, *J. Mol. Liq.* 265 (2018) 299–306.
- [20] L. Marin, A. Bejan, S. Shova, Phenothiazine based co-crystals with enhanced luminescence, *Dyes Pigments* 175 (2020) 108164.
- [21] T. Cristofolini, M. Dalmina, J.A. Sierra, A.A. Silva, A.A. Pasa, F. Pittella, T.B. Creczynski-Pasa, Multifunctional hybrid nanoparticles as magnetic delivery systems for siRNA targeting the HER2 gene in breast cancer cells, *Mat. Sci. Eng. C* 109 (2020) 110555.
- [22] R. Catana, M. Barboiu, I. Moleavin, L. Clima, A. Rotaru, E.L. Ursu, M. Pinteala, Dynamic constitutional frameworks for DNA biomimetic recognition, *Chem. Comm.* 51 (2015) 2021–2024.
- [23] A. Janse van Rensburg, N.H. Davies, A. Oosthuysen, C. Chokoza, P. Zilla, D. Bezuidenhout, Improved vascularization of porous scaffolds through growth factor delivery from heparinized polyethylene glycol hydrogels, *Acta Biomater.* 49 (2017) 89–100.
- [24] T.T. Le, D. Kim, Folate-PEG/Hyd-curcumin/C18-g-PSI micelles for site specific delivery of curcumin to colon cancer cells via Wnt/ β -catenin signaling pathway, *Mat. Sci. Eng. C* 101 (2019) 464–471.
- [25] M. Zamani, M. Aghajanzadeh, K. Rostamizadeh, H. Kheiri Manjili, M. Fridoni, H. Danafar, In vivo study of poly (ethylene glycol)-poly (caprolactone)-modified folic acid nanocarriers as a pH responsive system for tumor-targeted co-delivery of tamoxifen and quercetin, *J Drug Deliv Sci Technol* 54 (2019) 101283.
- [26] H. Kheiri Manjili, H. Malvandi, M. Sajjad Mousavi, E. Attari, H. Danafar, In vitro and in vivo delivery of artemisinin loaded PCL-PEG-PCL micelles and its pharmacokinetic study, *Artif Cell Nanomed B* 46 (2017) 926–936.
- [27] K. Rostamizadeh, M. Manafi, H. Nosrati, H. Kheiri Manjili, H. Danafar, Methotrexate-conjugated mPEG-PCL copolymers: a novel approach for dual triggered drug delivery, *New J. Chem.* 43 (2019) 10658.
- [28] A.A. D'souza, R. Shegokar, Polyethylene glycol (PEG): a versatile polymer for pharmaceutical applications, *Expert. Opin. Drug Del.* 13 (2016) 1257–1275.
- [29] A. Johansson, P. Kollman, S. Rothenberg, J. McKelvey, Hydrogen bonding ability of the amide group, *J. Am. Chem. Soc.* 96 (1974) 3794–3800.
- [30] K. Molcanov, B. Kojić-Prodić, N. Raos, Analysis of the less common hydrogen bonds involving ester oxygen sp³ atoms as acceptors in the crystal structures of small organic molecules, *Acta Crystallogr. B.* 60 (2004) 424–432.
- [31] C. Bissantz, B. Kuhn, M. Stahl, A medicinal chemist's guide to molecular interactions, *J. Med. Chem.* 53 (2010) 5061–5084.
- [32] G.M. Dumitriu, A. Ghinet, E. Bicu, B. Rigo, J. Dubois, A. Farce, D. Beleu, Peptide chemistry applied to a new family of phenothiazine-containing inhibitors of human farnesyltransferase, *Bioorg. Med. Chem. Lett.* 24 (2014) 3180–3185.
- [33] D. Beleu, C. Dumea, A. Samson, A. Farce, J. Dubois, E. Bicu, A. Ghinet, New farnesyltransferase inhibitors in the phenothiazine series, *Bioorg. Med. Chem. Lett.* 22 (2012) 4517–4522.
- [34] B.S. Lele, M.A. Gore, M.G. Kulkarni, Direct esterification of poly (ethylene glycol) with amino acid hydrochlorides, *Synthetic Commun* 29 (1999) 1727–1739.
- [35] S.A. Hart, K.C. Chandra Bikram, K.N. Subbaiyan, A.P. Karr, F. D'Souza, Phenothiazine-sensitized organic solar cells: effect of dye anchor group positioning on the cell performance, *J. Am. Chem. Soc.* 4 (2012) 5813–5820.
- [36] D. Ailincăi, C. Farcau, E. Paslaru, L. Marin, PDLC composites based on polyvinyl borate matrix – a promising pathway towards biomedical engineering, *Liq. Cryst.* 43 (2016) 1973–1985.
- [37] A. Herrmann, Dynamic combinatorial/covalent chemistry: a tool to read, generate and modulate the bioactivity of compounds and compound mixtures, *Chem. Soc. Rev.* 43 (2014) 1899–1933.
- [38] M. Liu, X. Zhang, B. Yang, F. Deng, J. Ji, Y. Yang, Z. Huang, X. Zhang, Y. Wei, Luminescence tunable fluorescent organic nanoparticles from polyethyleneimine and maltose: facile preparation and bioimaging applications, *RSC Adv.* 4 (2014) 22294–22298.
- [39] A.C.B. Rodrigues, J. Pina, W. Dong, M. Forster, U. Scherf, J.S. Seixas de Melo, Aggregation-induced emission in phenothiazine –TPE and –TPAN polymers, *Macromolecules* 51 (2018) 8501–8512.
- [40] A. Dinache, M. Boni, M.L. Pascu, Phenothiazine derivatives interaction with laser radiation, *Rom. Rep. Phys.* 65 (2013) 1078–1091.
- [41] B.E. Risteen, A. Blake, M.A. McBride, C. Rosu, J.O. Park, M. Srinivasarao, P.S. Russo, E. Reichmanis, Enhanced alignment of water-soluble Polythiophene using cellulose nanocrystals as a liquid crystal template, *Biomacromolecules* 8 (2017) 1556–1562.
- [42] A. Liess, A. Lv, A. Arjona-Esteban, D. Bialas, A.M. Krause, V. Stepanenko, M. Stolte, F. Würthner, Exciton coupling of merocyanine dyes from H- to J-type in the solid state by crystal engineering, *Nano Lett.* 17 (2017) 1719–1726.
- [43] S.B. Anantharaman, D. Messmer, A. Sadeghpour, S. Salentinig, F. Nüesch, J. Heier, Excitonic channels from bio-inspired templated supramolecular assembly of J-aggregate nanowires, *Nanoscale* 11 (2019) 6929–6938.
- [44] L. Marin, D. Ailincăi, M. Calin, D. Stan, C.A. Constantinescu, L. Ursu, F. Doroftei, P. Mariana, B.C. Simionescu, M. Barboiu, Dynamic frameworks for DNA transfection, *ACS Biomater. Sci. Eng.* 2 (2016) 104–111.
- [45] I. Mushtaq, Z. Akhter, F.U. Shah, Tunable self-assembled nanostructures of electroactive pegylated tetra(aniline) based ABA triblock structures in aqueous medium, *Frontiers in Chemistry* 7 (2019) 518.
- [46] X. Ma, R. Sun, J. Cheng, J. Liu, F. Gou, H. Xiang, X. Zhou, Fluorescence aggregation-caused quenching versus aggregation-induced emission: a visual teaching technology for undergraduate chemistry students, *J. Chem. Educ.* 93 (2016) 345–350.
- [47] R. Jiang, L. Huang, M. Liu, F. Deng, H. Huang, J. Tian, Y. Wen, Q. Cao, X. Zhang, Y. Wei, Ultrafast microwave-assisted multicomponent tandem polymerization for rapid fabrication of AIE-active fluorescent polymeric nanoparticles and their potential utilization for biological imaging, *Mat. Sci. Eng. C.* 83 (2018) 115–120.
- [48] L. Wang, Q. Xia, Z. Zhang, J. Qu, R. Liu, Precise design and synthesis of an AIE fluorophore with near-infrared emission for cellular bioimaging, *Mat. Sci. Eng. C* 93 (2018) 399–406.
- [49] S.C. Owena, D.P.Y. Chana, M.S. Shoichet, Polymeric micelle stability, *Nano Today* 7 (2012) 53–65.
- [50] S. Mahesh, K.C. Tang, M. Raj, Amide bond activation of biological molecules, *Molecules* 23 (2018) 2615.
- [51] M. Hamidreza Kheiri, N. Alimohammadi, H. Danafar, Preparation of biocompatible copolymeric micelles as a carrier of atorvastatin and rosuvastatin for potential anticancer activity study, *Pharm. Dev. Technol.* 24 (2018) 303–313.
- [52] M. Zamani, K. Rostamizadeh, H. Kheiri Manjili, H. Danafar, In vitro and in vivo biocompatibility study of folate-lysine PEG-PCL as nanocarrier for targeted breast cancer drug delivery, *Eur. Polym. J.* 103 (2018) 260–270.
- [53] D. Zámbo, Sz. Pothorsky, D.F. Brougham, A. Deák, Aggregation kinetics and cluster structure of amino-PEG covered gold nanoparticles, *RSC Adv.* 6 (2016) 27151–27157.
- [54] L. Guerrini, R.A. Alvarez-Puebla, N. Pazos-Perez, Surface modifications of nanoparticles for stability in biological fluids materials, *Materials* 11 (2018) 1154.
- [55] P.A. de Faria, F. Bettanin, R.L. Cunha, E.J. Paredes-Gamero, P. Homem-de-Mello, I.L. Nantes, T. Rodrigues, Cytotoxicity of phenothiazine derivatives associated with mitochondrial dysfunction: a structure-activity investigation, *Toxicology* 330 (2015) 44–54.
- [56] D. Mehta, N. Leong, V.M. McLeod, B.D. Kelly, R. Pathak, D.J. Owen, C.J.H. Porter, L.M. Kaminskas, Reducing dendrimer generation and PEG chain length increases drug release and promotes anti-cancer activity of PEGylated polylysine dendrimers conjugated with doxorubicin via a cathepsin-cleavable peptide linker, *Mol. Pharm.* 15 (2018) 4568–4576.
- [57] L. Tang, X. Yang, Q. Yin, K. Cai, H. Wang, I. Chaudhury, C. Yao, Q. Zhou, M. Kwon, J.A. Hartman, I.T. Dobrucki, L.W. Dobrucki, L.B. Borst, S. Lezmi, W.G. Helfferich, A.L. Ferguson, T.M. Fan, J. Chenga, Investigating the optimal size of anticancer nanomedicine, *Proc. Natl. Acad. Sci. U. S. A.* 111 (2014) 15344–15349.
- [58] F. Li, T. Jiang, Q. Li, X. Ling, Camptothecin (CPT) and its derivatives are known to target topoisomerase I (Top1) as their mechanism of action: did we miss something in CPT analogue molecular targets for treating human disease such as cancer? *Am. J. Cancer Res.* 7 (2017) 2350–2394.
- [59] X. Guoa, L. Shenc, Y. Tong, J. Zhang, G. Wu, Q. He, S. Yu, X. Ye, L. Zou, Z. Zhang, X.Y. Lian, Antitumor activity of caffeic acid 3,4-dihydroxyphenethyl ester and its pharmacokinetic and metabolic properties, *Phytomedicine* 20 (2013) 904–912.
- [60] W. Olejarz, M. Wrzosek, M. Józwiak, E. Grosicka-Maciąg, P. Roszkowski, A. Filipiek, A. Cychol, G. Nowicka, M. Struga, Synthesis and anticancer effects of α -lipoic ester of alloxanthoxyletin, *Med. Chem. Res.* 28 (2019) 788–796.
- [61] S. Yang, M. Liu, H. Xiang, S. Yang, Synthesis and in vitro antitumor evaluation of betulin acid ester derivatives as novel apoptosis inducers, *Eur. J. Med. Chem.* 102 (2015) 249–255.
- [62] C. Xu, T. Deng, M. Fan, W. Lv, J. Liu, B. Yu, Synthesis and in vitro antitumor evaluation of dihydroartemisinin-cinnamic acid ester derivatives, *Eur. J. Med. Chem.* 107 (2016) 192–203.
- [63] K. Ne, W. Fr, M. Sd, G.E., D. Sj, C. Mw, A. Nj, H. Wj, G. Rp, L. Tj, More, protein farnesyltransferase inhibitors block the growth of ras-dependent tumors in nude-mice, *P. Natl. Acad. Sci. USA.* 91 (1994) 9141–9145.
- [64] V. Sereikaitė, T.M.T. Jensen, C.R.O. Bartling, P. Jemth, S.A. Pless, K. Strømgaard, Probing backbone hydrogen bonds in proteins by amide-to-ester mutations, *ChemBiochem* 19 (2018) 2136–2145.